Hindawi
Advances in Civil Engineering
Volume 2018, Article ID 4308084, 12 pages
https://doi.org/10.1155/2018/4308084

Research Article

Uniaxial Compressive Test of High Ductile Fiber-Reinforced Concrete and Damage Constitutive Model

Mingke Deng, Jiaojiao Pan, and Xingwen Liang

School of Civil Engineering, Xi'an University of Architecture and Technology, Xi'an 710055, China

Correspondence should be addressed to Mingke Deng; dengmingke@126.com

Received 5 August 2017; Revised 18 November 2017; Accepted 23 November 2017; Published 25 February 2018

Academic Editor: Chiara Bedon

It has been widely recognized that the constitutive model plays an essential role in engineering application of high ductile fiber-reinforced concrete (HDC). In this research, uniaxial compressive tests were conducted on nine groups of HDC specimens with different mixture ratios and one group of mortar matrix specimens as comparison, discussing the effect of fiber content, water-cement ratio, fly ash content, and sand-binder ratio. According to the characteristics of stress-strain curve of HDC under uniaxial compression, a damage constitutive model was proposed by introducing two damage threshold parameters and then was compared with other existing models. Results indicated that the damage model curves suggested in this paper were best consistent with experimental curves and substantially demonstrate the damage evolution process as well as the cracking resistance effect of fiber bridging stress.

1. Introduction

High ductile fiber-reinforced concrete (HDC) [1], just like engineered cementitious composites (ECCs) [2, 3], is also a kind of high performance fiber-reinforced cementitious composite (HPFRCC) [4, 5], which is composed primarily of cement, fine aggregate, and fiber. HDC is manufactured based on the designed theory of micromechanics and fracture mechanics and can be characterized by pseudostrain hardening and multiple cracking behaviors when subjected to tensile loading. Recently, due to its excellent durability, high toughness, and remarkable damage resistance capacity, HDC has been widely utilized in civil engineering, particularly in the flexure and shear-dominated members, such as coupling beams, low-rise walls, and beam-column joints [6–9]. Findings suggested that HDC can effectively enhance the structural performance and improve the shear strength, energy dissipation, and damage tolerance of members.

In the engineering application mentioned above, there are stringent requirements on mechanical behavior and stress-strain relationship of HDC. Therefore, many investigations have been carried out to investigate the compressive property and constitutive relationship of HDC. Fakharifar et al. [10] statistically evaluated the effect of fiber content on compressive and flexural strengths through adequate tests and found that the first crack and failure strength as well as mechanical properties were enhanced by increasing the fiber content. Ma et al. [11] suggested that excessive amounts of fly ash tend to decrease the compressive strength though ductility improved with fly ash content. Due to the vital role of the constitutive model in the design and analysis of structure, Li and Liu [12] and Xu et al. [13], respectively, built the constitutive models based on the stress-strain curves of HDC under uniaxial compression. However, the abovementioned models neglected the microcracks and microvoids in HDC and thus cannot reflect the damage evolution of HDC under uniaxial compression. So, it is necessary to build a constitutive model considering the initial damage in HDC.

Over the past 30 years, damage mechanics has been widely employed to describe the failure process for traditional building material. The existing researches indicated that damage theory is a reasonable way to evaluate the constitutive relationship of concrete due to its powerful theoretical framework [14–20]. Furthermore, owing to its solid foundation for irreversible thermodynamics and

Table 1: Properties of PVA fiber.

Length (mm)	Diameter (μm)	Length-diameter ratio	Tensile strength (MPa)	Modulus of elasticity (GPa)	Elongation (%)	Density (g/cm^3)
12	39	0.31×10^3	1600	40	7	1.3

relevant consideration of physical mechanisms, continuum damage mechanics serves as an effective method to the research of the stress-strain relationships of concrete and rock in a comprehensive way [21–26]. Xue et al. [27] introduced the damage threshold parameters and established a damage constitutive model of steel fiber-reinforced concrete reflecting the linear elastic behavior under low stress. Therefore, damage mechanics can be used to derive the constitutive model of HDC. The toughness and deformability of HDC under uniaxial compression can be significantly improved for the lateral restraint effect of the fiber bridging stress inside the matrix, which has obvious difference with concrete [1]. The researchers [21–27] primarily focused on the concrete and steel fiber-reinforced concrete, both of which can be classified as a brittle material. Consequently, their models are unable to reflect the damage accumulation and constitutive relationship of HDC under the uniaxial compressive stress state.

The present research reports on uniaxial compressive tests of HDC with different mixture ratios, discussing the effect of fiber bridging stress on the failure mode. In addition, it includes an investigation into the influence laws of ingredients, such as polyvinyl alcohol (PVA) fiber volume, water-cement ratio, fly ash content, and sand-binder ratio, on the characteristic points of HDC stress-strain curves. Besides, based on the features of experimental curves, this paper established a modified damage constitutive model by introducing two damage threshold parameters γ and β and then compared this damage model with the existing models. It should be stressed that the model proposed in this paper describes the damage evolution process and provides a theoretical basis for the nonlinear analysis of components and the ductility design of the structure.

2. Experimental Program

2.1. Material. The ingredients of HDC adopted in the test are cement (PO 42.5R), fly ash, fine river sand, PVA fiber, mineral admixtures, water, and superplasticizer. Table 1 presents the mechanical properties of PVA fiber. Nine groups of HDC and one group of mortar matrix with different mix proportions were designed and three identical specimens were cast for each group. The dimension of prismatic specimens was 100 mm × 100 mm × 300 mm, and the mixture ratios are given in Table 2. Test parameters in this paper included PVA content (1%, 1.5%, and 2%), water-cement ratio (0.26, 0.29, and 0.32), fly ash content (40%, 50%, and 60%), and sand-binder ratio (0.24, 0.36, and 0.48).

2.2. Testing Method. Figure 1 gives the schematic diagram of test setup. To obtain the strain-stress curve of HDC under uniaxial compression, the linear variable differential transformers (LVDTs) were installed between both ends of the specimen and measured the whole longitudinal deformation of the specimen. The load was applied through a 500t microcomputer-controlled electrohydraulic servo

Table 2: Mix design for experimental program.

Code	PVA content (%)	Water-binder ratio	Fly ash content (%)	Sand-binder ratio
1	0	0.29	50	0.36
2	1.0	0.29	50	0.36
3	1.5	0.29	50	0.36
4	2.0	0.29	50	0.36
5	2.0	0.26	50	0.36
6	2.0	0.32	50	0.36
7	2.0	0.29	60	0.36
8	2.0	0.29	40	0.36
9	2.0	0.29	50	0.24
10	2.0	0.29	50	0.48

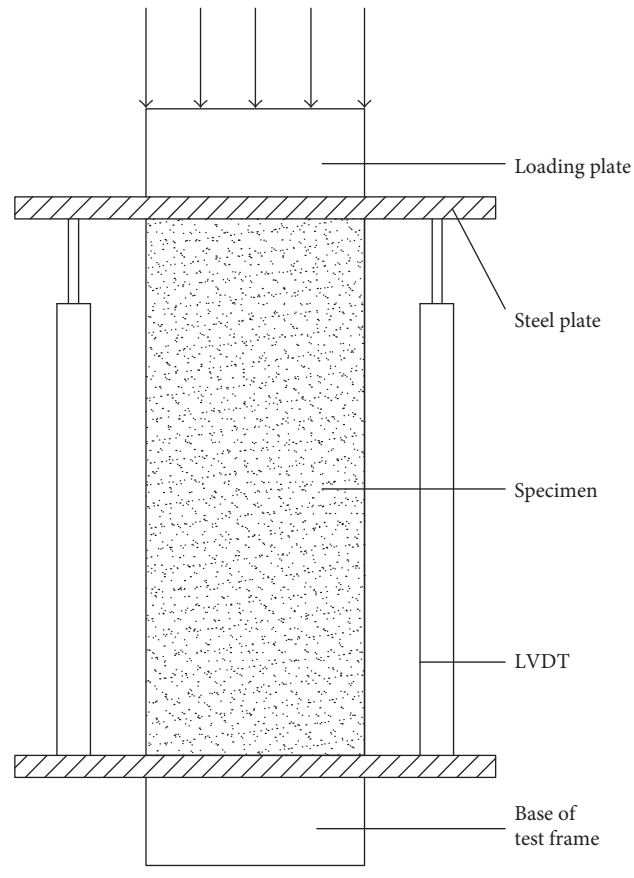

Figure 1: The schematic diagram of test setup.

(a) (b) (c) (d) (e)

Figure 2: Typical failure mode of specimens. (a) Matrix, (b) HDC-2, (c) HDC-4, (d) HDC-5, and (e) HDC-6.

compressive testing machine. The loading was controlled by displacement at a rate of 0.5 mm/min, and the data were collected through the TDS602 Data Logger.

3. Results and Discussion

3.1. Failure Mode. Figure 2 shows the typical failure modes of specimens. The brittle splitting failure occurred for the matrix specimen, and the specimen was divided into several prisms at the ultimate stage (Figure 2(a)). In contrast, the HDC specimens remained intact at the softening stage, and finally a major inclined shear crack formed along the specimens (Figures 2(b)–2(e)), which agreed with the conclusions in research [28]. The shear failure mode of HDC specimens exhibited obvious ductility compared with the matrix specimen.

The fiber bridging effect can be used to explain this phenomenon. During the failure process of HDC under uniaxial compression, the fiber bridging stress effectively restrains the lateral deformation of specimens (Figure 3), and thus, the appearance and propagation of longitudinal cracks are delayed. The fibers are pulled out or pulled apart when the lateral tensile deformation exceeds the ultimate tensile strain of HDC, leading to the inefficacy of the lateral constraining force. Thus, longitudinal cracks will appear at the weakest part of specimens, which will run through the specimens from top to bottom and eventually form a major crack. During the failure process of specimens, there is obvious dislocation at both sides of the major diagonal crack. The specimens are still in good condition and have residual bearing capacity due to the fiber bridging effect even if they are damaged. Conclusions can be drawn that, due to the lateral restraint effect of fiber bridging stress, the damage and failure processes of HDC under uniaxial compression are quite different from those of concrete.

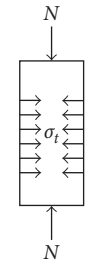

Figure 3: Lateral restraint effect of fiber bridging stress.

3.2. Uniaxial Compressive Stress-Strain Curves and Characteristic Points. Uniaxial compressive stress-strain curves obtained through the test are shown in Figure 4. Characteristic points of the stress-strain curves of specimens together with the corresponding values of stress and strain are given in Table 3. It can be known from Figure 4 and Table 3 that the corresponding peak strain of mortar matrix (mixture ratio 1) is 0.0021, which is quite close to that of concrete. The uniaxial compressive stress-strain curve of HDC is a unimodal curve, and the peak strain of 9 groups of HDC specimens is 2.61–3.15 times that of mortar matrix. This indicates that the deformability of HDC specimens has been significantly improved before peak load. Once over the peak load, the mortar matrix immediately loses bearing capacity. Although HDC specimen also has a sudden drop of load, there is always 10–20% residual bearing capacity in the specimen when large compressive strain appears.

3.3. Effect of Factors on the Characteristic Points of Stress-Strain Curves. According to the test results in Table 3, the effects of four factors (fiber content, water-binder ratio, fly

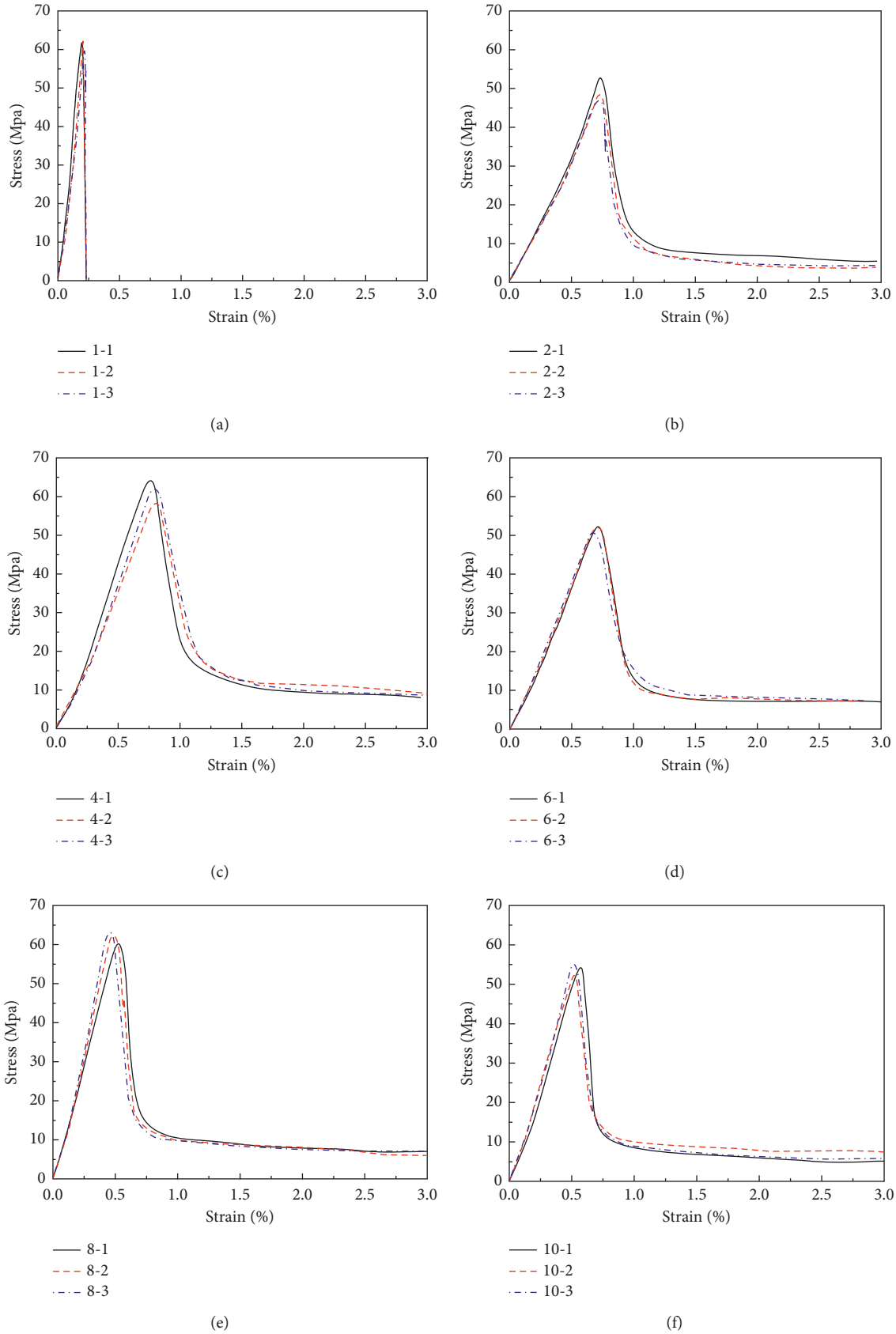

Figure 4: Typical uniaxial compression stress-strain curves of HDC. (a) Matrix, (b) HDC-2, (c) HDC-4, (d) HDC-6, (e) HDC-8, and (f) HDC-10.

Table 3: Characteristic points of HDC stress-strain curve.

Code	P_m (kN)	σ_0 (MPa)	$\sigma_{0.2}$ (MPa)	ε_0 (10^{-3})	$\varepsilon_{0.85}$ (10^{-3})	$\varepsilon_{0.5}$ (10^{-3})	$\varepsilon_{0.2}$ (10^{-3})
1	630.55	63.06	—	2.13	—	—	—
2	502.78	50.28	10.06	5.69	6.02	6.67	8.64
3	568.50	56.85	11.37	6.01	6.66	6.95	11.28
4	622.52	62.25	12.45	6.72	8.01	9.32	14.07
5	560.35	56.04	11.21	6.33	7.05	7.69	11.16
6	528.38	52.84	10.57	6.52	7.88	9.52	12.76
7	536.35	53.64	10.73	6.34	7.90	9.47	13.80
8	644.32	64.43	12.89	5.61	6.41	6.94	8.87
9	519.60	51.96	10.39	6.48	8.14	9.23	13.57
10	560.05	56.01	11.20	5.56	6.05	6.66	8.10

Note: (1) P_m is peak load; σ_0 is peak stress; ε_0 is the strain corresponding to peak stress; (2) $\sigma_{0.2}$ is the stress value when the stress declines to 20% of peak stress; (3) $\varepsilon_{0.85}$, $\varepsilon_{0.5}$, and $\varepsilon_{0.2}$ are the corresponding ultimate compressive strain values when the stress declines to 85%, 50%, and 20% of peak stress, respectively.

ash content, and sand-binder ratio) on the characteristic points of stress-strain curves of HDC under uniaxial compression (Figure 5) can be found out. The analyses on four influencing factors are as follows.

3.3.1. Fiber Content. As shown in Figure 5(a), the peak stress σ_0 of the HDC specimen increases with the increase in fiber content. Besides, $\varepsilon_{0.85}$, $\varepsilon_{0.5}$, and $\varepsilon_{0.2}$ increase by 33.06%, 39.73%, and 62.85%, respectively, as fiber content increases to 2% from 1%. It can be attributed to the disordered short fibers preventing the appearance and development of microcracks. As a result, the compressive strength and deformability of HDC specimens were improved.

3.3.2. Water-Binder Ratio. From Figure 5(b), it can be seen that the ultimate strain and compressive strength of HDC specimens increase as water-binder ratio increases from 0.26 to 0.29 and then decline as the water-binder ratio increases to 0.32. It suggested that the ratio 0.29 was more effective than others in terms of enhancing the compressive behavior of HDC. This phenomenon appeared for the reason that the increased water-binder ratio improved the workability of the mixture, leading to the more uniform distribution of fibers inside the matrix. Consequently, the toughness and cracking resistance of HDC enhanced. However, the high water-binder ratio reduced the compressive strength of HDC.

3.3.3. Fly Ash Content. As shown in Figure 5(c), the peak strain of specimens demonstrates a significant rise when the fly ash content increases from 40% to 50% and a slight reduction when the fly ash content increases from 50% to 60%, together with the ultimate compressive strain. The cause is that fly ash can improve the interfacial bond properties between fibers and matrix, thus preventing excessive fiber rupture and enhancing the toughness of HDC [1]. It should also be noted that the maximum stress declines with the increase in the fly ash content. Thus, the fly ash content should be limited, considering enough compressive strength.

3.3.4. Sand-Binder Ratio. The deformation capacity of specimens improves when the sand-binder ratio rises from 0.24 to 0.36. It drops instead of rising continually when the sand-binder ratio increases to 0.48, which can be attributed to the fact that the friction force between fibers and matrix increases due to the excessive sand-binder ratio. As a result, most of the fibers are pulled apart, and the tensile deformability of the material declines, thus reducing the ultimate compressive strain of specimens. From Figure 5(d), it also can be known that the maximum stress of specimens with a sand-binder ratio of 0.36 is higher than that of specimens with sand-binder ratios of 0.24 and 0.48. Hence, the ratio 0.36 was most favorable to improving the compressive strength and strain capacity of HDC.

4. Damage Constitutive Model of HDC under Uniaxial Compression

4.1. Establishment of Damage Constitutive Model. Let A be the cross-sectional area of the material under undamaged condition and $\widetilde{A}$ be the effective bearing area decreased by the damage. Then, the damage variable D can be expressed as

$$D = \frac{A - \widetilde{A}}{A} = 1 - \frac{\widetilde{A}}{A}. \tag{1}$$

The effective bearing area can be expressed as

$$\widetilde{A} = (1 - D)A. \tag{2}$$

Let $\widetilde{\sigma}$ be the ratio of external load F to the effective loading area. Then,

$$\widetilde{\sigma} = \frac{F}{\widetilde{A}} = \frac{F}{(1 - D)A} = \frac{\sigma}{(1 - D)}, \tag{3}$$

where σ is the nominal stress on the cross section of components, and $\sigma = F/A$.

According to the equivalent strain hypothesis theory proposed by Lemaitre [29], the constitutive relation of damaged material can be derived from the constitutive equation of the nondestructive material under uniaxial stress by replacing the nominal stress of the constitutive relation of

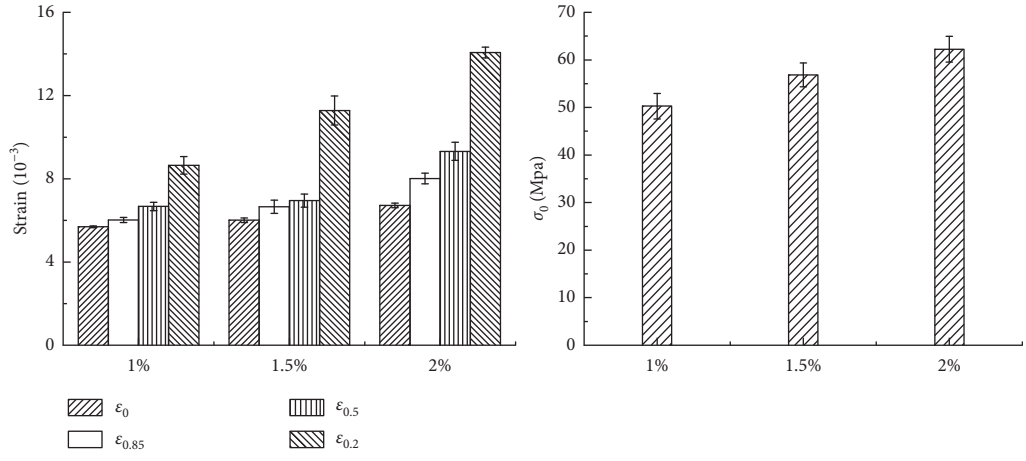

(a)

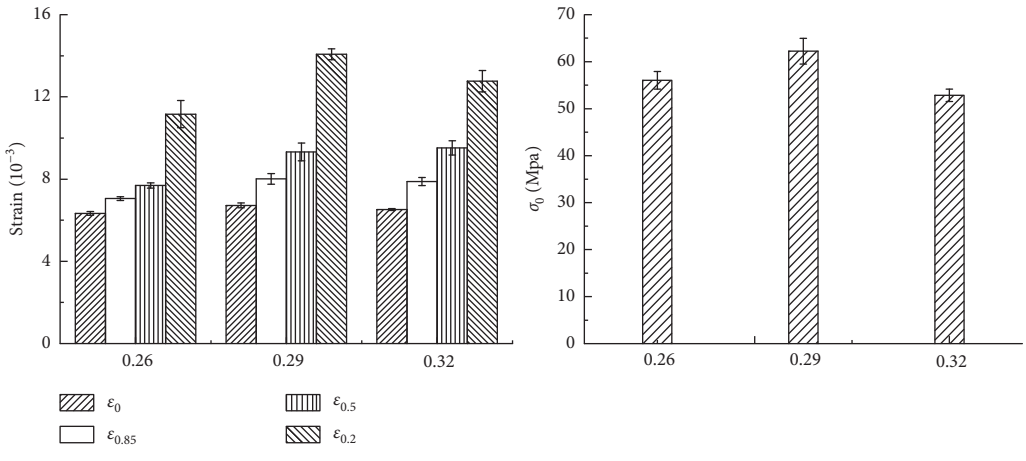

(b)

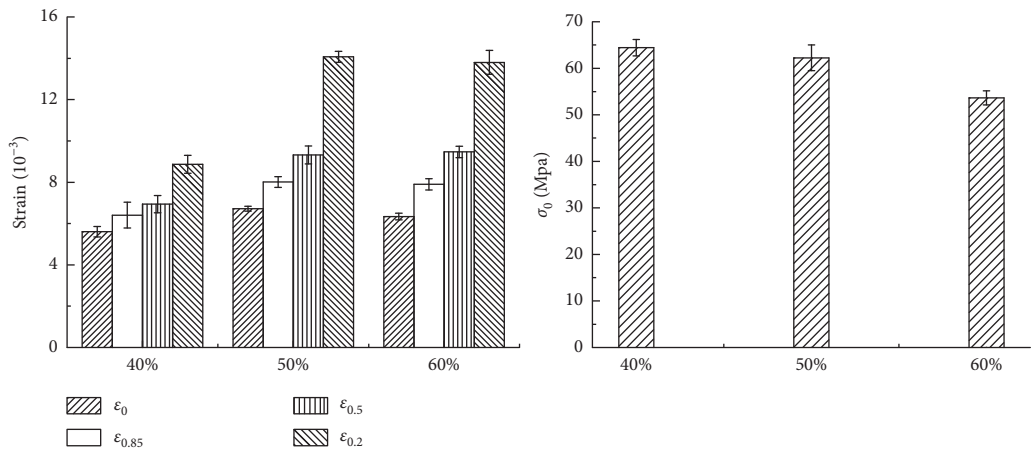

(c)

Figure 5: Continued.

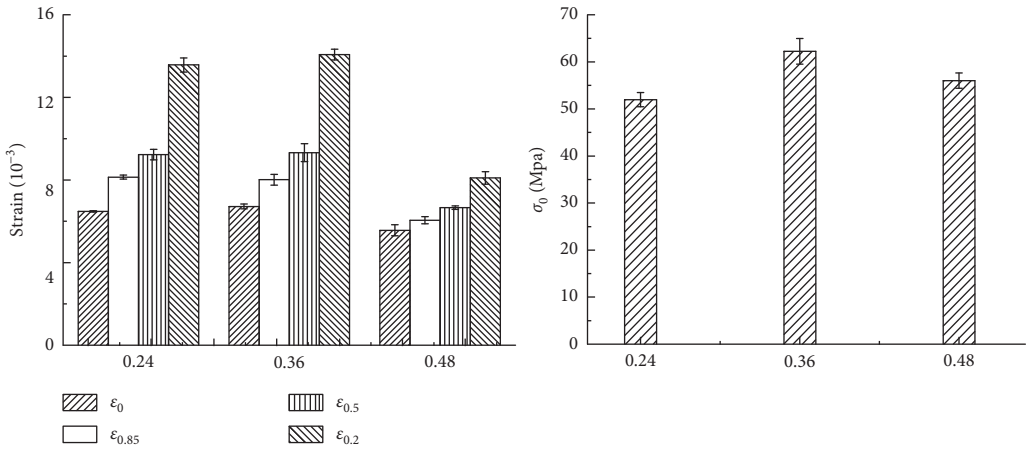

(d)

Figure 5: Influence of factors on the characteristic points of stress-strain curves of HDC. (a) Fiber content. (b) Water-binder ratio. (c) Fly ash content. (d) Sand-binder ratio.

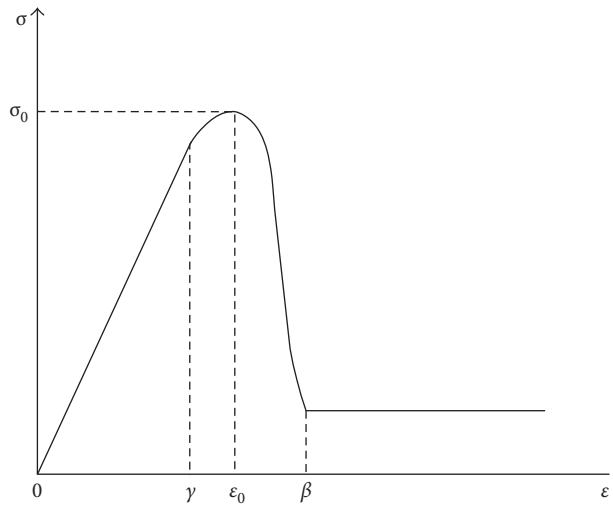

Figure 6: Stress-strain curve of HDC.

the undamaged material with the effective stress. Let ε be the damaged elastic strain, and then the damage constitutive relation of the material is ($\widetilde{\sigma} = E\varepsilon$)

$$\sigma = E(1 - D)\varepsilon. \tag{4}$$

4.2. Derivation of Damage Evolution Equation. As for the damage fracture of rock and concrete, the literature [25, 26] suggests that the damage variable D of the material fulfills Weibull distribution. Thus,

$$D = 1 - \exp\left[-\left(\frac{\varepsilon}{\eta}\right)^m\right], \tag{5}$$

where m and η (nonnegative numbers), respectively, are the shape parameter and scale parameter.

From the stress-strain curve of the HDC specimen, it should be noted that the linear elastic stage elongates and the strain corresponding to the initial damage is enlarged. In addition, the damage of HDC tends to be stable, and there is 10%–20% residual bearing capacity in specimens when the strain exceeds a certain value. Based on the above analysis, two damage thresholds γ and β are introduced in this paper to build the damage constitutive model of HDC. γ is the initial point at the nonlinear ascent stage, and β is the initial point at the residual stage. Then, the damage variable can be expressed as follows:

Damage variable:

$$D = \begin{cases} 0 & (\varepsilon < \gamma) \\ 1 - \exp\left[-\left(\frac{\varepsilon - \gamma}{\eta}\right)^m\right] & (\gamma \le \varepsilon \le \beta) \\ D_u & (\varepsilon > \beta), \end{cases} \tag{6}$$

Table 4: Parameters of damage constitutive model.

Code	m	η ($\times 10^{-3}$)	γ/ε_0	β/ε_0	D		Correlation coefficient of model		
					ε_0	β	New proposal	Li	Xu
2	5.78	0.26	0.80	1.21	0.03	0.89	0.983	0.987	0.962
3	4.36	0.27	0.82	1.27	0.04	0.85	0.975	0.972	0.947
4	2.56	0.38	0.84	1.43	0.06	0.83	0.982	0.982	0.948
5	5.22	0.22	0.82	1.20	0.03	0.87	0.978	0.980	0.947
6	3.94	0.28	0.82	1.28	0.04	0.85	0.985	0.982	0.957
7	2.92	0.29	0.84	1.38	0.05	0.84	0.977	0.980	0.941
8	3.74	0.19	0.84	1.29	0.04	0.87	0.991	0.993	0.974
9	2.63	0.30	0.82	1.41	0.06	0.79	0.991	0.986	0.964
10	4.60	0.19	0.83	1.26	0.04	0.88	0.990	0.989	0.978
μ	—	—	0.83	1.30	0.05	0.85	0.984	0.983	0.958
δ	—	—	0.013	0.060	0.243	0.035	0.006	0.006	0.013

where D_u is the damage value when the strain ε is equal to β, that is, the maximum damage variable.

Damage constitutive model:

$$\sigma = \begin{cases} E\varepsilon & (\varepsilon < \gamma) \\ E(1-D)\varepsilon & (\gamma \le \varepsilon \le \beta) \\ (1-D_u)\sigma_0 & (\varepsilon > \beta). \end{cases} \tag{7}$$

4.3. Determination of Model Parameter. The shape of the stress-strain curve of HDC under uniaxial compression can be obtained (Figure 6).

As seen in Figure 6, the stress-strain curve of HDC meets the following boundary conditions:

(1) $\varepsilon = 0, \sigma = 0$

(2) $\varepsilon = 0, d\sigma/d\varepsilon = E$ (E is the initial elastic modulus)

(3) $\sigma = \sigma_0, \varepsilon = \varepsilon_0$

(4) $\sigma = \sigma_0, d\sigma/d\varepsilon = 0$

Through the features (1), (2), (3), and (4) of stress-strain curves of HDC, the parameters (m, η) can be calculated as follows:

$$m = \frac{\varepsilon_0 - \gamma}{\varepsilon_0} \frac{1}{\ln(E\varepsilon_0/\sigma_0)}, \tag{8}$$

$$\eta = \frac{\varepsilon_0 - \gamma}{(\varepsilon_0 - \gamma/m\varepsilon_0)^{1/m}}. \tag{9}$$

4.4. Comparisons of Experimental Curves and Model Curves. The parameters of HDC damage constitutive model under uniaxial compression was calculated, and the results of model parameters and damage variable (at point ε_0 and β) are listed in Table 4. The parameters m, η can be worked out through expressions (8) and (9). μ and δ are the average and coefficient of variation of parameters.

As shown in Table 4, the value γ/ε_0 of HDC is about 0.83. This indicates that the elastic section of HDC stress-strain curves elongates and the damage resistance ability is stronger. Let γ be $0.8\varepsilon_0$ and β be $1.3\varepsilon_0$ so as to substitute the two damage thresholds into expression (7). Then, the damage constitutive model of HDC under uniaxial compression can be worked out. Then, there is

$$\sigma = \begin{cases} E\varepsilon & (\varepsilon < 0.8\varepsilon_0) \\ E\varepsilon \exp\left[-\left(\frac{\varepsilon-\gamma}{\eta}\right)^m\right] & (0.8\varepsilon_0 \le \varepsilon < 1.3\varepsilon_0) \\ (1-D_u)\sigma_0 & (\varepsilon \ge 1.3\varepsilon_0). \end{cases} \tag{10}$$

Li and Liu [12] and Xu et al. [13] suggested the constitutive models of this material in which the damage in HDC was not considered. The descent stage of curve adopted the same equation in these models, whereas the ascent stage used rational fraction equation and polynomial equation, respectively. Those are as follows:

The descent stage:

$$y = \frac{x}{B(x-1)^2 + x} \quad (x \ge 1). \tag{11}$$

The ascent stage:

Li's model:

$$y = \frac{Ax - x^2}{1 + (A-2)x} \quad (0 \le x < 1). \tag{12}$$

Xu's model:

$$y = C_1 + C_2 x + C_3 x^2 + C_4 x^3 \quad (0 \le x < 1), \tag{13}$$

where $x = \varepsilon/\varepsilon_0, y = \sigma/\sigma_0$, and A, B, C_1, C_2, C_3, C_4 are the fitting coefficients.

This research, respectively, calculated the correlation coefficients of three model curves and the experimental curves as shown in Table 4. The fitting coefficients A, B, C_1, C_2, C_3, C_4 in Li's model and Xu's model were

Table 5: Fitting coefficients.

Code	A	B	C_1	C_2	C_3	C_4
2-1	1.034	37.134	0.0047	0.8317	−0.1147	0.2940
2-2	1.074	43.974	0.0100	0.7613	0.2643	−0.0267
2-3	1.073	43.258	0.0135	0.7258	0.2227	0.0569
3-1	1.078	27.678	0.0070	0.4882	1.0398	−0.5319
3-2	1.091	32.823	0.0059	0.3222	1.6317	−0.9484
3-3	1.080	28.726	0.0131	0.6201	0.3015	0.0776
4-1	1.109	20.536	0.0065	0.4160	1.6010	−1.0100
4-2	1.091	20.647	0.0197	0.5249	1.0022	−0.5326
4-3	1.083	16.407	0.0137	0.3248	1.4095	−0.7329
5-1	1.024	42.674	0.0029	0.6888	−0.0087	0.3471
5-2	1.032	38.564	0.0000	0.7332	−0.2785	0.5767
5-3	1.035	42.354	0.0056	0.3815	1.0399	−0.4061
6-1	1.087	20.680	0.0052	0.6321	0.7937	−0.4198
6-2	1.093	15.564	−0.0022	0.8249	0.3049	−0.1172
6-3	1.119	14.659	0.0085	0.6399	0.8406	−0.4703
7-1	1.093	12.386	−0.0009	0.6471	0.5464	−0.1774
7-2	1.103	14.471	0.0076	0.5708	0.9070	−0.4720
7-3	1.104	12.851	0.0172	0.3625	1.0927	−0.4394
8-1	1.075	35.291	0.0023	0.7590	0.6093	−0.3669
8-2	1.080	39.523	0.0062	0.5423	1.1401	−0.6759
8-3	1.073	33.200	0.0139	0.3904	1.2833	−0.6612
9-1	1.099	14.372	0.0115	0.5952	0.7945	−0.3913
9-2	1.094	15.626	0.0100	0.4324	1.4337	−0.8676
9-3	1.093	17.578	0.0028	0.6649	0.4437	−0.0906
10-1	1.055	39.618	0.0118	0.5097	0.9268	−0.4402
10-2	1.058	42.618	0.0006	0.6400	0.8168	−0.4523
10-3	1.070	35.641	0.0005	0.6940	0.4779	−0.1649

given in Table 5. Figure 7 describes the comparisons of experimental curves and constitutive model curves. The relation curves between the damage variable D and strain are shown in Figure 8, and then the damage evolution process of HDC under uniaxial compression is observed. Compared with the Li's and Xu's models, the damage model suggested in this paper had the following features:

(1) The damage model curves are in best agreement with experimental curves reflecting the characteristic of linear elastic deformation and the residual bearing capacity of HDC which can be attributed to the restraint effect of fiber bridging stress. However, the ascent stage of Xu's model curves had great difference with the experimental curves whose correlation coefficient is smaller than those in the damage model and Li's model.

(2) The damage model describes the damage development process and the effect of toughness and crack resistance of fiber in this period, whereas Li's and Xu's models cannot reflect the damage evolution of HDC under uniaxial compression.

(3) As fiber content increases, the parameter m of the damage constitutive model decreases, whereas η constantly increases. Therefore, the area enclosed by the stress-strain curve also increases gradually. It suggested that the energy dissipation capacity of HDC was improved with added fiber content.

(4) When strain reaches the damage threshold β, the damage variable D is about 0.85 (smaller than 1.0). HDC is still not damaged completely when the deformation is large. It suggests that fibers can delay the damage propagation of concrete, just like the fact that the fiber bridging stress can delay the crack propagation.

5. Conclusions

This research dealt with the effects of ingredients on the compressive properties of HDC. The damage constitutive

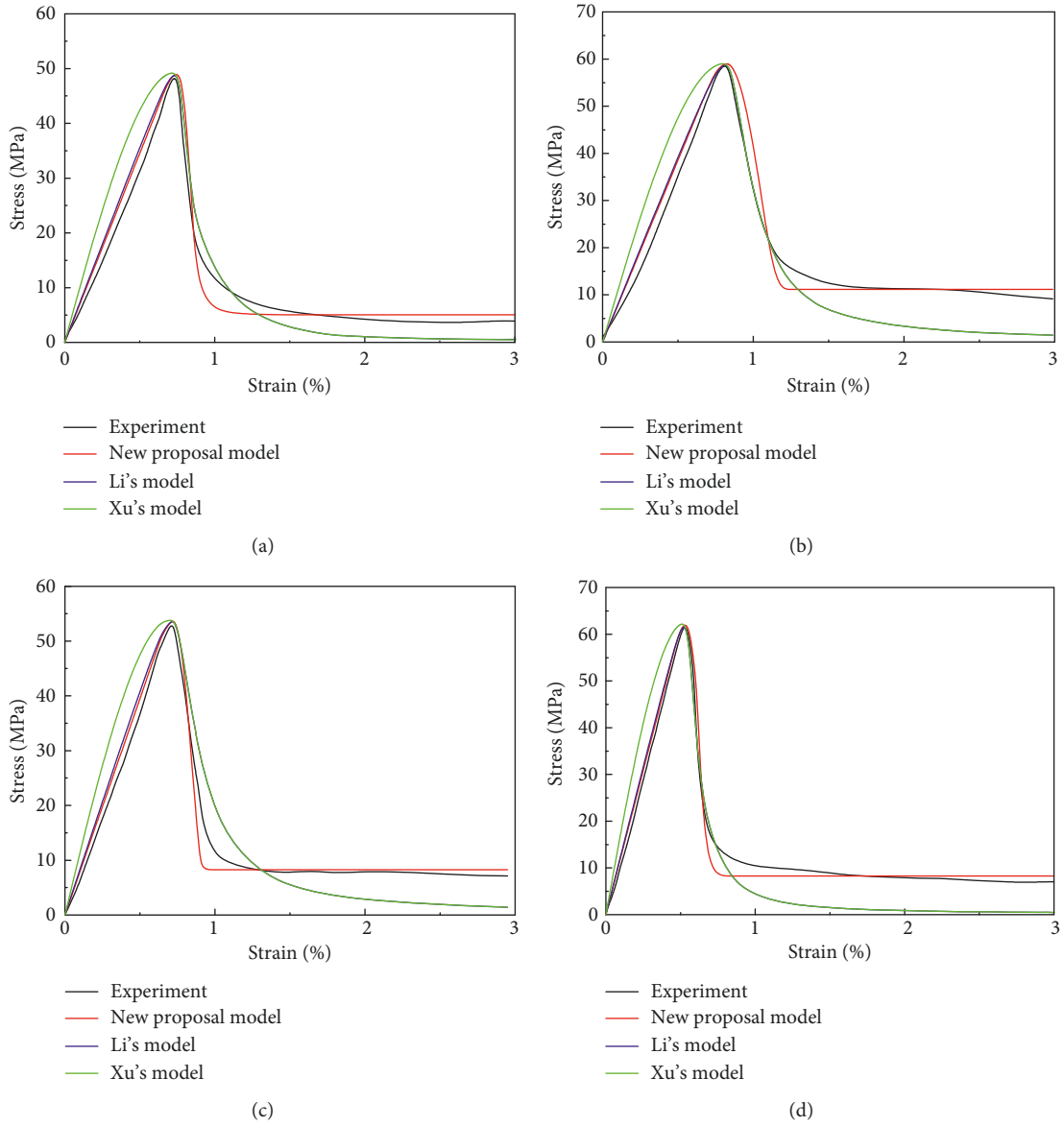

Figure 7: Comparisons of experimental curves and model curves. (a) HDC 2-2, (b) HDC 4-2, (c) HDC 6-2, and (d) HDC 8-1.

model was established by using two damage threshold parameters γ and β based on the stress-strain relationship attaining from uniaxial compressive tests. The following conclusions can be drawn:

(1) The mortar matrix specimen fails in brittle split under uniaxial compression and is divided into several prisms after failure. In contrast, the ductile shear failure occurs for the HDC specimens due to the lateral confinement effect of fiber bridging stress.

(2) The stress-strain curve of HDC under uniaxial compression is a unimodal curve, and the peak deformation is 2.61–3.15 times that of mortar matrix. Besides, the HDC specimens still remain intact and have 10–20% residual bearing capacity at the ultimate stage.

(3) Based on the features of stress-strain curves of HDC under uniaxial compression, two damage threshold parameters are introduced and then a damage constitutive model is built. Besides, the damage model curves fit best with the experimental curves and reflect the damage development process of HDC compared with two existing models.

(4) As the fiber content increases, the parameter m of the damage constitutive model gradually decreases, whereas η constantly increases. It suggests that the energy dissipation capacity of HDC is improved with the added fiber content.

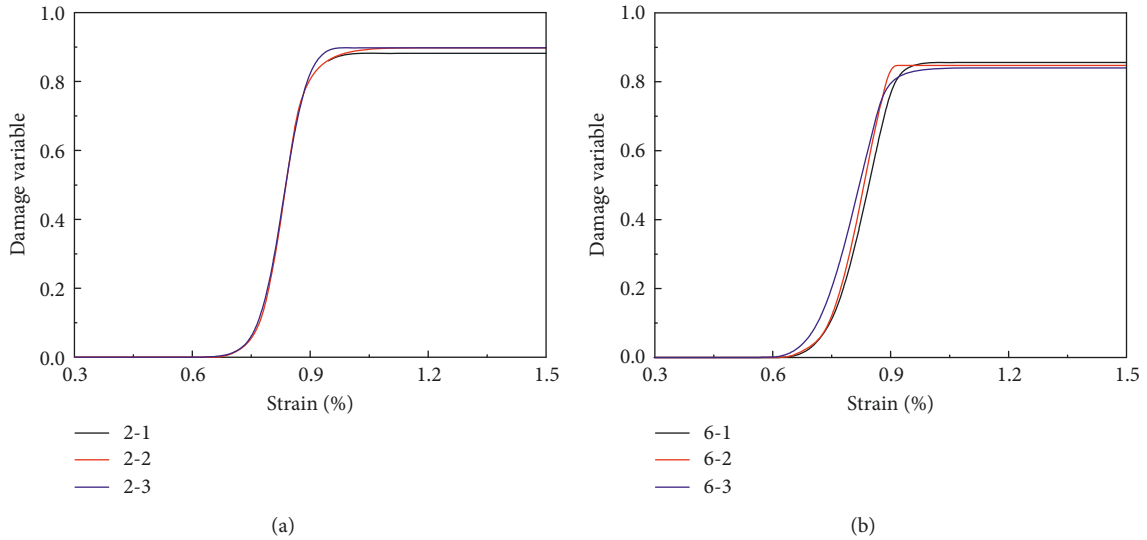

Figure 8: Relation curves between damage variable and strain: (a) HDC 2 and (b) HDC 6.

Conflicts of Interest

The authors declare that there are no conflicts of interest regarding the publication of this paper.

Acknowledgments

This research is funded by the Natural Science Foundation of China (No. 51578445) and Key Laboratory Project in Shaanxi Province Education Department (No. 15JS048). The authors would like to thank the laboratory teachers from the School of Civil Engineering for their help with specimen fabrication and testing.

References

[1] M. K. Deng, J. Han, H. B. Liu, M. Qin, and X. W. Liang, "Analysis of compressive toughness and deformability of High Ductile Fiber Reinforced Concrete," *Advances in Materials Science and Engineering*, vol. 2015, Article ID 384902, 7 pages, 2015.

[2] V. C. Li and H. C. Wu, "Conditions for pseudo strain-hardening in fiber reinforced brittle matrix composites," *Applied Mechanics Reviews*, vol. 45, no. 8, pp. 390–398, 1992.

[3] S. Wang and V. C. Li, "High early strength Engineered Cementitious Composites," *ACI Material Journal*, vol. 103, no. 2, pp. 97–105, 2006.

[4] K. G. Kuder and S. P. Shah, "Processing of high-performance fiber-reinforced cement-based composites," *Construction and Building Materials*, vol. 24, no. 2, pp. 181–186, 2010.

[5] G. J. Parra-Montesinos, "High-performance fiber-reinforced cement composites: an alternative for seismic design of structures," *ACI Structure Journal*, vol. 102, no. 5, pp. 668–675, 2005.

[6] G. Fischer and V. C. Li, "Influence of matrix ductility on tension-stiffening behavior of steel reinforced Engineered Cementitious Composites (ECC)," *ACI Structure Journal*, vol. 99, no. 1, pp. 104–111, 2002.

[7] G. Fischer and V. C. Li, "Effect of matrix ductility on deformation behavior of steel reinforced ecc flexural members under reversed cyclic loading conditions," *ACI Structure Journal*, vol. 99, no. 6, pp. 781–790, 2011.

[8] G. Fischer and V. C. Li, "Deformation behavior of fiber-reinforced polymer reinforced Engineered Cementitious Composite (ECC) flexural members under reversed cyclic loading conditions," *ACI Structure Journal*, vol. 100, no. 1, pp. 25–35, 2003.

[9] S. Qian, Y. Y. Kim, and V. C. Li, "Influence of concrete material ductility on shear response of stud connections," *ACI Materials Journal*, vol. 103, no. 1, pp. 60–66, 2006.

[10] M. Fakharifar, A. Dalvand, M. Arezoumandi, M. Sharbatdar, G. Chen, and A. Kheyroddin, "Mechanical properties of high performance fiber reinforced cementitious composites," *Construction and Building Materials*, vol. 71, pp. 510–520, 2014.

[11] H. Ma, S. Qian, Z. Zhang, Z. Lin, and V. C. Li, "Tailoring Engineered Cementitious Composites with local ingredients," *Construction and Building Materials*, vol. 101, pp. 584–595, 2015.

[12] Y. Li and Z. J. Liu, "Study on mechanical performance and constitutive equation of high toughness PVA-FRCC under uniaxial compression," *Journal of Building Materials*, vol. 17, no. 4, pp. 606–612, 2014, in Chinese.

[13] S. L. Xu, X. R. Can, and Y. H. Zhang, "Experimental measurement and analysis of the axial compressive stress-strain curve of ultra high toughness cementitious composites," *Civil Engineering Journal*, vol. 42, no. 11, pp. 79–85, 2009, in Chinese.

[14] G. Swoboda, X. P. Shen, and L. Rosas, "Damage model for jointed rock mass and its application to tunneling," *Computers and Geotechnics*, vol. 22, no. 3-4, pp. 183–203, 1998.

[15] W. Suaris, C. Ouyang, and V. M. Fernando, "Damage model for cyclic loading of concrete," *Journal of Engineering Mechanics*, vol. 116, no. 5, pp. 1020–1035, 1990.

[16] D. Krajcinovic and M. A. G. Silva, "Statistical aspects of the continuous damage theory," *International Journal of Solids and Structures*, vol. 18, no. 7, pp. 551–562, 1982.

[17] C. Mazzotti and M. Savoia, "Nonlinear creep damage model for concrete under uniaxial compression," *Journal of Engineering Mechanics*, vol. 129, no. 9, pp. 1065–1075, 2003.

[18] K. E. Loland, "Continuous damage model for load-response estimation of concrete," *Cement and Concrete Research*, vol. 10, no. 3, pp. 395–402, 1980.

[19] D. Krajcinovic, "Constitutive equations for damaging materials," *Journal of Applied Mechanics*, vol. 50, no. 2, pp. 355–360, 1983.

[20] J. Mazars and J. Lemaitre, *Application of Continuous Damage Mechanics to Strain and Fracture Behavior of Concrete*, pp. 375–378, Springer, Evanston, IL, USA, 1984.

[21] M. H. Liu and Y. F. Wang, "Damage constitutive model of ash concrete under freeze-thaw cycles," *Journal of Materials in Civil Engineering*, vol. 24, no. 9, pp. 1165–1174, 2012.

[22] H. Zhao, C. J. Shi, M. H. Zhao, and X. B. Li, "Statistical damage constitutive model for rocks considering residual strength," *International Journal of Geomechanics*, vol. 17, no. 1, p. 04016033, 2017.

[23] T. Yu, "Statistical damage constitutive model of quasi-brittle materials," *Journal of Aerospace Engineering*, vol. 22, no. 1, pp. 95–100, 2009.

[24] F. Leng and G. Wu, "A thermodynamics-based damage constitutive model of concrete," *European Journal of Environmental and Civil Engineering*, vol. 17, no. 1, pp. s83–s102, 2013.

[25] Z. L. Wang, Y. S. Liu, and R. F. Shen, "Stress–strain relationship of steel fiber-reinforced concrete under dynamic compression," *Construction and Building Materials*, vol. 22, no. 5, pp. 811–819, 2008.

[26] R. Hameed, A. Sellier, A. Turatsinze, and F. Duprat, "Damage model for concrete reinforced with sliding metallic fibers," *International Journal of Mechanics and Materials in Design*, vol. 7, no. 1, pp. 83–97, 2011.

[27] Y. L. Xue, S. L. Li, F. Lin, and H. B. Xu, "Study of damage constitutive model of SFRC considering effect of damage threshold," *Rock and Soil Mechanics*, vol. 30, no. 7, pp. 1987–1992, 2009, in Chinese.

[28] J. J. Zhou, J. L. Pan, and C. K. Y. Leung, "Mechanical behavior of fiber-reinforced Engineering Cementitious Composites in uniaxial compression," *Journal of Materials in Civil Engineering*, vol. 27, no. 1, p. 04014111, 2015.

[29] J. Lemaitre, "How to use damage mechanics," *Nuclear Engineering and Design*, vol. 80, no. 2, pp. 233–245, 1984.